J. Fluid Mech. (1979), *vol.* 90, *part* 3, *pp.* 509–529
Printed in Great Britain

On the scaling of stress-driven entrainment experiments

By JAMES F. PRICE

Graduate School of Oceanography, University of Rhode Island, Kingston

(Received 23 February 1978 and in revised form 9 August 1978)

The entrainment experiments of Kato & Phillips (1969) and Kantha, Phillips & Azad (1977) (hereafter KP and KPA) are analysed to demonstrate a more general and effective scaling of the entrainment observations. The preferred scaling is

$$V^{-1} dh/dt = E(R_v),$$

where h is the mixed-layer depth, V is the mean velocity of the mixed layer, $R_v = B/V^2$ and B is the total mixed-layer buoyancy. This scaling effectively collapses entrainment data taken at various h/L, where L is the tank width, and in cases in which the interior is density stratified (KP) or homogeneous (KPA). The entrainment law $E(R_v)$ is computed from the KP and KPA observations using the conservation equations for mean momentum and buoyancy. A side-wall drag term is included in the momentum conservation equation. In the range $0{\cdot}5 < R_v < 1{\cdot}0$, which includes nearly all of the KP, KPA data, $E \simeq 5 \times 10^{-4} R_v^{-4}$. This is very similar to the entrainment law followed by a surface half-jet (Ellison & Turner 1959) and by the wind-driven ocean surface mixed layer (Price, Mooers & Van Leer 1978).

The analysis shows that, when forcing is steady, R_v is quasi-steady and, provided that side-wall drag is not large, $R_v \simeq 0{\cdot}6$ over a wide range of $R_\tau = B/U_*^2$, where U_* is the friction velocity of the imposed stress. In the absence of side-wall drag (vanishing h/L) the conservation of momentum then leads to $U_*^{-1} dh/dt = n(0{\cdot}6)^{\frac{1}{2}} R_\tau^{-\frac{1}{2}}$, where $n = \frac{1}{2}$ or 1 if the interior is linearly stratified or homogeneous. The KP, KPA data show this dependence throughout the range $17 < R_\tau < 160$ where the effect of side-wall drag is negligible or can be removed by a linear extrapolation. This result, together with the form and magnitude of the observed side-wall effect, suggests that mean momentum conservation is a key constraint upon the entrainment rate in the KP, KPA experiments.

1. Introduction

Deepening of a mixed layer by turbulent entrainment generally cannot be modelled explicitly and must be parameterized. The relevant variables of a parameterization can be guessed by physical intuition. The functional form must be fixed from precise observations. Adequate observations are difficult to acquire from natural systems because unwanted processes such as advection and diabatic heating often obscure entrainment. Laboratory observations made under controlled conditions (no advection, simple and repeatable forcing and initial conditions) are relatively precise and inexpensive. Laboratory studies have therefore played a central role in development of the parameterizations and physical concepts of entrainment (Turner 1973).

Laboratory studies also have their hazards. The special geometry of an apparatus

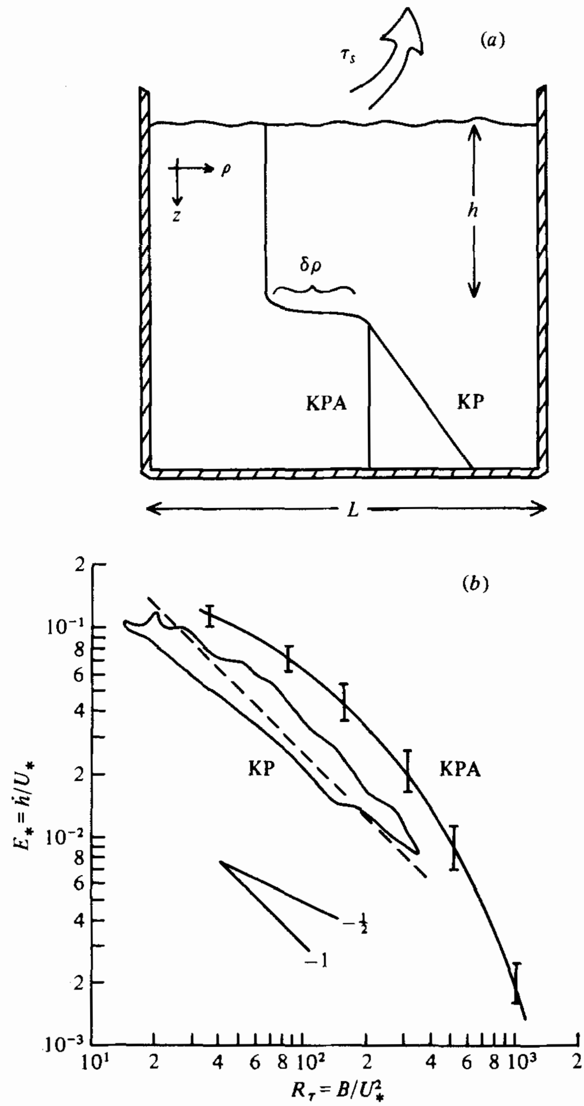

FIGURE 1. (a) Channel cross-section of the annular tank used by KP and KPA. The interior was linearly stratified in the KP experiment and homogeneous in the KPA experiment. A constant stress τ_s was applied at the surface by a rotating screen. (b) The results $E_*(R_\tau)$ of the KP, KPA experiments. KP data are continuously distributed within the cloud outlined here. The aspect ratio h/L varied from 0·2 to 0·6. The dashed line is the KP fit, $E_* = 2{\cdot}5\, R_\tau^{-1}$. KPA data were taken only at the discrete values of R_τ shown by the error bars. The data shown here are for $h/L = 0{\cdot}25$.

and the special procedure followed in an experiment may cause a result to be highly specific even if the process modelled is rather general. In this paper the stress-driven entrainment experiments of Kato & Phillips (1969) (hereafter KP) and Kantha, Phillips & Azad (1977) (KPA) are analysed to demonstrate a more effective scaling of the entrainment observations and to examine the effect of the tank side walls. The aim is to provide a more generally applicable form of the KP, KPA experimental results. The detailed mechanics of the entrainment process is not considered here.

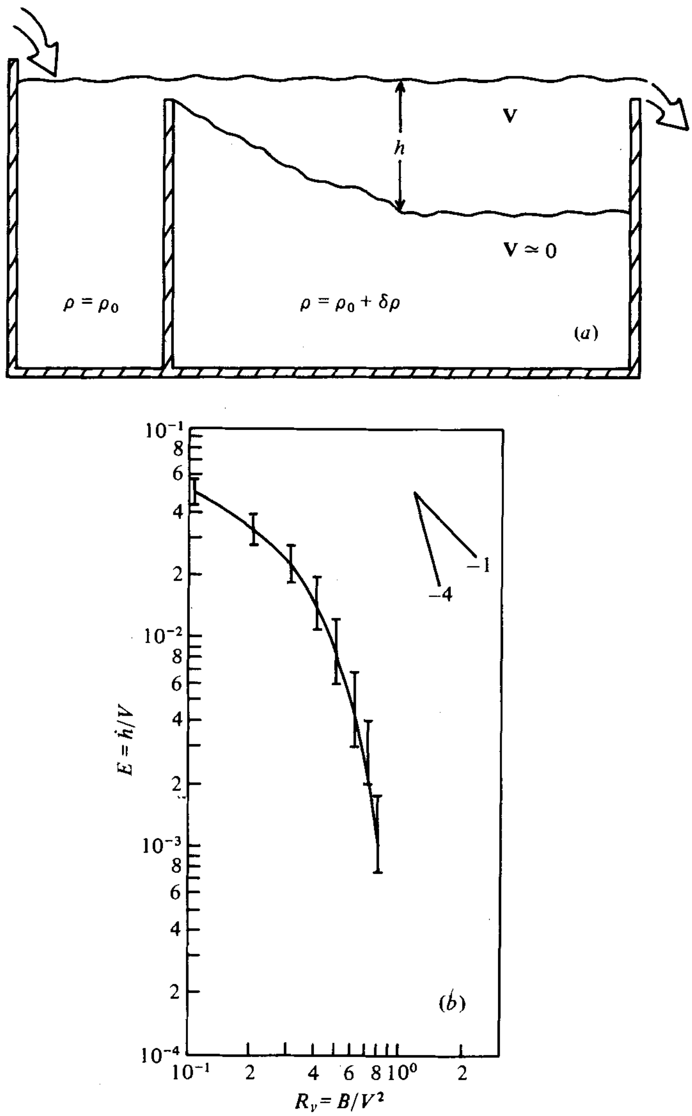

FIGURE 2. (a) Schematic of the ET surface half-jet experiment. The entrainment velocity was $\dot{h} = V dh/dx$, where x is the downstream co-ordinate. (b) The ET experimental result, $\dot{h}/V = E(R_v)$. In general, the velocity V must be the velocity difference $V - V_i$, where V_i is the velocity in the interior. In all cases considered here, $V_i \cong 0$.

KP and KPA modelled quasi-steady wind-driven deepening of the ocean surface mixed layer. The observed entrainment velocity $\dot{h}$, where h is the mixed-layer depth and the dot indicates an ordinary time derivative, was scaled using external, bulk parameters: the friction velocity $U_* = (\tau_s/\rho)^{\frac{1}{2}}$ of the imposed stress, the mixed-layer depth and the mixed-layer buoyancy $b = g\delta\rho/\rho$, where $\delta\rho$ is the density difference across the base of the mixed layer and g is the acceleration due to gravity (figure 1a). Entrainment data were expressed non-dimensionally as $\dot{h}/U_* = E_*(R_\tau)$, where $R_\tau = B/U_*^2$ is a bulk Richardson number and $B = bh$ is the total mixed-layer buoyancy. The form of the entrainment law E_* was the essential result (figure 1b).

It is convenient and desirable to express experimental results in terms of external parameters. However, scaling with U_* does not collapse the KP, KPA data; E_* depends not only upon R_τ but also upon the aspect ratio h/L, where L is the tank width, and upon the form of density stratification. The fundamental point of this paper is that the scaling $\dot{h}/V = E(R_v)$, where V is the mean velocity of the mixed layer, does effectively collapse the data. The entrainment law E is somewhat general in that it holds in time-dependent cases and describes entrainment in other superficially different mixed-layer flows.

An indication that mean-velocity scaling might be preferred for the KP, KPA experiments came from an analysis of oceanic wind-driven mixed-layer deepening by Price *et al.* (1978). The oceanic cases were in the R_τ regime of the experiments but, unlike the experiments, were highly time dependent because of the earth's rotation and time-variable wind stress. The relevant scaling velocity for the oceanic cases was found to be the mean velocity and clearly not the friction velocity. The entrainment law was found to be similar to the result of the Ellison & Turner (1959) (hereafter ET) experiment, in which entrainment by a surface half-jet was determined as a function of the directly observed R_v (figure 2). The ET experiment is apparently the only relevant experiment in which mean-velocity scaling has been used.† It is shown here that the KP, KPA experiments follow essentially the same entrainment law.

The notion of scaling the KP, KPA results with V is not new. Phillips (1977) suggested that V was the relevant scaling velocity because shear-flow instabilities at the base of the mixed layer appear to initiate the entrainment process. Pollard, Rhines & Thompson (1973) have shown that their bulk model, which employs mean-velocity scaling, is consistent with some of the KP data. Mellor & Durbin (1975) have shown that their second-order turbulence closure model is also consistent with some of the KP data and with mean-velocity scaling. The present study is new in that side-wall drag and the form of density stratification are considered explicitly and because the data are used to determine E directly.

Outline of this paper

The mean velocity was not accurately measured by KP or KPA and must be computed for this analysis. The model momentum conservation equation and its consequence are discussed in § 2. In § 3 the model is used to compute $E(R_v)$ for the KP, KPA experiments. This demonstrates that the KP, KPA experimental results are consistent with those of ET and Price *et al.* (1978) but provides little insight. Therefore in § 4 the problem is worked in reverse; $E(R_v)$ is used to predict E_* and V, which are compared in detail with the experimental observations. In § 5 the KP data are used to compute E_* at $h/L = 0$. In § 6 the results are summarized and interpreted.

The KP, KPA experiments are reviewed in the remainder of this section. Readers familiar with the experiments may wish to skip this but should note equation (3a).

† Moore & Long (1971) used the depth of their tank, not the mixed-layer depth, as the length scale in their bulk Richardson number. Lofquist (1960) studied entrainment by a bottom half-jet at very large R_v.

Review of the KP, KPA experiments

The KP, KPA experiments were conducted in the same annular tank (figure 1*a*) and followed identical procedures; a constant stress τ_s was applied at the surface of a stratified fluid by a rotating screen, and the mixed-layer depth h and the screen velocity U_s were observed in time. Viscosity was assumed to be unimportant at the relatively high Reynolds numbers achieved in the experiments and no time scale was relevant because entrainment data were analysed only if the flow was quasi-steady. Under those conditions the entrainment velocity may be written in terms of external variables:

$$\dot{h}/U_* = E_*(U_*, h, \delta\rho/\rho, g, L). \tag{1}$$

Under the Boussinesq approximation the fractional density difference is important only where multiplied by g and (1) may be rewritten as

$$\dot{h}/U_* = E_*(R_\tau, h/L). \tag{2}$$

The KP, KPA experiments differed only in the form of the density stratification. KP used linear stratification; KPA used two-layer stratification. A rather general density profile which includes both cases is (with $z = 0$ at the surface and positive down and omitting a constant term)

$$\rho = \begin{cases} \alpha h_0^m - \delta\rho_0 & \text{for} \quad z < h_0, \\ \alpha z^m & \text{for} \quad z \geqslant h_0, \end{cases}$$

where $m \geqslant 0$, and h_0 and $\delta\rho_0$ are the initial mixed-layer depth and density difference. The linearly stratified KP case corresponds to $h_0 = 0$, $\alpha = \partial\rho/\partial z =$ constant and $m = 1$; the KPA case corresponds to h_0 and $\delta\rho_0$ specified, $\alpha =$ reference density and $m = 0$. The dependence of the total mixed-layer buoyancy upon h is the important property of the density profile. For the generalized profile,

$$B(h) = h_0 \frac{g}{\rho}\left(\delta\rho_0 - \alpha\frac{m}{m+1}h_0^m\right) + \alpha\frac{g}{\rho}\frac{m}{m+1}h^{m+1}, \tag{3a}$$

where the first term is called the excess total buoyancy of the profile and the second term is the increase in B due to mixed-layer deepening. In the KP case

$$B = \tfrac{1}{2}N^2h^2, \tag{3b}$$

where $N^2 = g/\rho\,(\partial\rho/\partial z)$ is the buoyancy frequency squared; hence B and thus R_τ increased with h during an experimental run. In the KPA case

$$B = gh_0\delta\rho_0/\rho = \text{constant}, \tag{3c}$$

thus $R_\tau =$ constant during an experimental run. R_τ was varied by using different values of the imposed stress and N^2 or $h_0\delta\rho_0$.

For most purposes E_* must be known at $h/L = 0$, i.e. in the limit of no side-wall effect. KP noted an anomalous decrease in the entrainment velocity which they attributed to a side-wall effect when h/L exceeded about 0·6. They attempted to exclude the contaminating side-wall effect by rejecting data for which $h/L > 0{\cdot}6$. KPA used a two-layer fluid specifically to isolate the side-wall effect. They argued that if R_τ was held constant then according to (2) the variation of E_* during an experimental run was attributable entirely to variation of h/L. Entrainment at $h/L = 0$ was inferred from observations made in the range $0{\cdot}35 < h/L < 0{\cdot}50$ by a subjective, linear extrapolation (observations were made at $h/L = 0{\cdot}25$ in several runs with $R_\tau < 300$).

At the same R_τ and h/L, E_* was a factor of 2 larger in the two-layer case than in the linearly stratified case (figure 1*b*). Apart from this the KP and KPA results were virtually identical over the range of common R_τ. KP fitted the line $E_* = 2{\cdot}5\,R_\tau^{-1}$ to their data. The slope of -1 was interpreted as showing a simple proportionality between turbulent energy dissipation ($\propto U_*^3$) and work against buoyancy ($\propto B\dot{h}$). This interpretation of the experimental result has been widely applied to modelling the energetics of entrainment in the atmosphere and ocean (e.g. Turner 1973, pp. 299–306).

2. A model of the KP, KPA experiments

The equation of momentum conservation for the mean or bulk velocity V is taken to be

$$\frac{d(hV)}{dt} = \frac{\tau_s}{\rho} - 2\frac{\tau_w h}{\rho L}, \tag{4}$$

where τ_w is the stress due to the side walls, ρ is a reference density and L is the channel width ($= 22{\cdot}8$ cm). The assumptions made in (4) and their justifications are as follows.

(i) The channel is assumed to be locally straight. KP noted a slight radial tilt of the interface but no violent secondary circulation due to channel curvature.

(ii) The Boussinesq approximation has been made for convenience. Analysis of a non-Boussinesq model indicates that this is satisfactory except at the very largest R_τ achieved by KPA, where it will result in a systematic overestimate of predicted entrainment. However, at very large R_τ the uncertainty in the parameterization of τ_w is more significant than the non-Boussinesq effect.

(iii) There is assumed to be no loss of momentum from the mixed layer except to the side walls. The interior was observed to remain virtually at rest until h approached the depth of the tank.

The side-wall stress is parameterized as

$$\tau_w = \rho C V^2. \tag{5}$$

The drag coefficient C is evaluated from the Blasius formula for turbulent channel flow (Schlichting 1968, p. 594):

$$C = 0{\cdot}04\,Re^{-\frac{1}{4}},$$

where $Re = VL/\nu$ is a Reynolds number and $\nu = 0{\cdot}01$ cm^2 s^{-1} is the molecular kinematic viscosity of water. A typical value of V is 25 cm s^{-1}, hence $Re = 6{\cdot}2 \times 10^4$ and

$$C = 2{\cdot}5 \times 10^{-3}. \tag{6}$$

It is sufficient for this study if C is correct to within about 30%. Dependence upon V is therefore ignored and C is taken to be fixed.

Using (5) and $\tau_s = \rho U_*^2$, the momentum balance (4) may be written as

$$d(hV)/dt = U_*^2(1 - 2CR_v^{-1}R_\tau h/L). \tag{7}$$

In the following section it will be shown that R_v varies from only approximately 0·5 to 1·0. In order to estimate roughly the side-wall drag term, R_v is taken as 0·75 and the right-hand side of (7) may be written in terms of external variables as

$$d(hV)/dt = U_*^2(1-\tfrac{1}{150}R_\tau h/L).$$

Side-wall drag is thus small if $R_\tau h/L \lesssim 15$ and appreciable if $R_\tau h/L \gtrsim 100$.

Without any further approximation (3*a*) and (7) may be used to calculate

$$E_* = \frac{\dot{h}}{U_*} = nR_v^{\frac{1}{2}}R_\tau^{-\frac{1}{2}}\left(1-2CR_v^{-1}R_\tau\frac{h}{L}\right)+\frac{n\dot{R}_v h}{2R_v U_*}, \tag{8}$$

where

$$n = 2/(\chi+2)$$

and

$$\chi = \frac{\alpha m h^{m+1}}{h_0\left(\delta\rho_0-\alpha\dfrac{m}{m+1}h_0^{m+1}\right)+\alpha\dfrac{m}{m+1}h^{m+1}}.$$

In the limit $h_0 \to 0$ (excess B negligible compared with the increase due to mixed-layer deepening), $\chi = m+1$; in the limit $m \to 0$ (excess B much larger than the increase due to mixed-layer deepening), $\chi = 0$. For the rather special stratification used in the KP, KPA experiments χ assumes these limiting values and

$$n = \begin{cases} \frac{1}{2} & \text{for KP,} \\ 1 & \text{for KPA.}\end{cases}$$

Given an entrainment law $E(R_v)$ which we wish to test, (8) predicts $E_*(R_\tau, h/L)$, which may be compared directly with observations of KP and KPA (§ 4). Even if the comparison of the predicted and observed E_* is very favourable, this approach cannot establish whether the entrainment law tested was unique, i.e. whether some other $E(R_v)$ would not do as well. Alternatively, given the KP, KPA data, (8) may be used to compute $E(R_v)$ directly. This is done in the following section.

3. Calculation of $E(R_v)$ from the KP, KPA data

Rearranging (8) to solve for $\dot{R}_v$, we have

$$\dot{R}_v = \frac{2\dot{h}}{nh}R_v + 4C\frac{U_*}{L}R_\tau^{\frac{1}{2}}R_v^{\frac{1}{2}} - 2\frac{U_*}{h}R_\tau^{-\frac{1}{2}}R_v^{\frac{3}{2}}, \tag{9}$$

which may be integrated to yield $R_v(t)$ given the observed $h(t)$ and known U_* and $B(h)$. Assuming that the stress is turned on at $t = 0$ when the fluid is at rest, a form of the initial condition which is convenient for numerical integration is

$$R_v(t_0) = B(h_0)h_0^2/U_*^4 t_0^2,$$

where t_0 is a time before entrainment begins (typically 15 s). The solution at $t \gg t_0$ is not sensitive to perturbations of the initial condition.

There is a consistent pattern in the behaviour of $R_v(t)$ (figure 3). R_v decreases rapidly during the transient phase at the beginning of an experimental run as V is accelerated by the imposed stress. R_v reaches a minimum as the entrainment rate

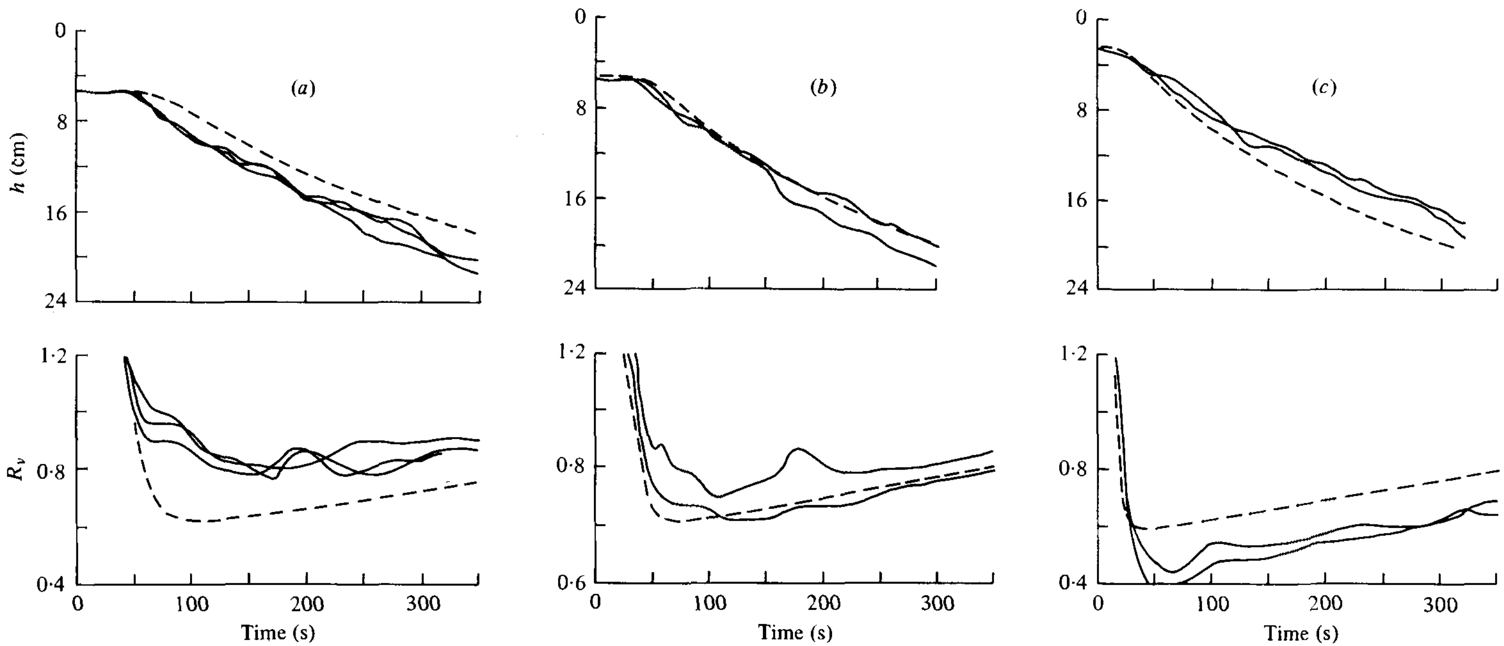

FIGURE 3. The top row is the observed $h(t)$ (solid lines) from KPA experimental runs with $R_\tau \simeq 145$. The bottom row is the corresponding $R_\nu(t)$ computed from (9). The dashed lines are model results discussed in the following section. (a) $h_0 = 5{\cdot}4$ cm, $U_* = 1{\cdot}41$ cm s^{-1}, $\delta\rho/\rho = 0{\cdot}055$, KPA runs 5, 6 and 34. (b) $h_0 = 5{\cdot}4$ cm, $U_* = 1{\cdot}93$ cm s^{-1}, $\delta\rho/\rho = 0{\cdot}090$, KPA runs 19 and 20. (c) $h_0 = 2{\cdot}7$ cm, $U_* = 1{\cdot}93$ cm s^{-1}, $\delta\rho/\rho = 0{\cdot}190$, KPA runs 31 and 44.

reaches a maximum and then slowly increases as the entrainment rate slowly decreases. The experimental runs of figure 3 have moderate to large side-wall drag ($30 \lesssim R_\tau h/L \lesssim 120$). In runs with less side-wall drag the rate of decrease of entrainment and increase of R_v is less than in figure 3. The value of R_v computed from (9) is sensitive to variations of h; a relatively large h gives a relatively large R_v by conservation of momentum.

After the transient phase and provided that side-wall drag is not large ($R_\tau h/L \lesssim 150$), R_v is quasi-steady,

$$\frac{n}{2}\frac{\dot{R}_v}{R_v} \ll \frac{\dot{h}}{h}, \tag{10}$$

and $\dot{R}_v$ may be neglected. Equation (9) is then algebraic and may be used to map observations from the external frame (R_τ, h/L, E_*) into (R_v, E). This has been done with data from KP runs 4 and 9 (these have extreme h/L at a given R_τ as discussed in the next section) and with all the KPA data with $R_\tau \lesssim 285$ and $h/L = 0{\cdot}5$ (figure 4). Several points at the beginning of both KP runs were deleted because R_v was decreasing rapidly and did not satisfy (10).

$E(R_v)$ for the KP, KPA experiments is very similar to the entrainment law found by ET for a surface half-jet. E decreases by approximately 1·5 orders of magnitude as R_v increases from 0·5 to 1·0. Most of the data fall in the range $0{\cdot}5 < R_v < 0{\cdot}8$. Data which have a larger R_v are primarily those with largest side-wall effect. An analytical representation of E in the range $R_v > 0{\cdot}5$ of interest here is

$$E = 5 \times 10^{-4} R_v^{-4}, \tag{11}$$

where the coefficient and the exponent have uncertainties of about 20%.

There is an overlap of KP and KPA data in figure 4 which suggests an effective collapse (cf. figure 1*b*). However, this result is not strongly supported because calculation of $E(R_v)$ from (9) exaggerates experimental scatter. Figure 4 is in any event difficult to interpret because both E and R_v are internal variables. We can verify that mean-velocity scaling does indeed collapse the KP, KPA data and learn the consequences of figure 4 by using (11) and its approximation to simulate the experiments.

4. Prediction of E_* and V

An approximate algebraic solution for quasi-steady E_*

It may be seen from (8) that the model predicts $E_*(R_\tau, h/L)$ if R_v and $\dot{R}_v$ are specified. The analysis of the previous section showed that when forcing was steady, R_v was quasi-steady (figure 3) and, provided that side-wall drag was not large, $R_v \simeq 0{\cdot}6$ over a rather wide range of R_τ (figure 4). This suggests that an approximate closure for the quasi-steady state is (cf. Pollard *et al.* 1973)

$$R_v = 0{\cdot}6, \tag{12}$$

independent of time and of R_τ. This is consistent with the oceanic cases of Price *et al.* (1978) which were in the range $R_\tau \approx 100$. Rory Thompson (personal communication)

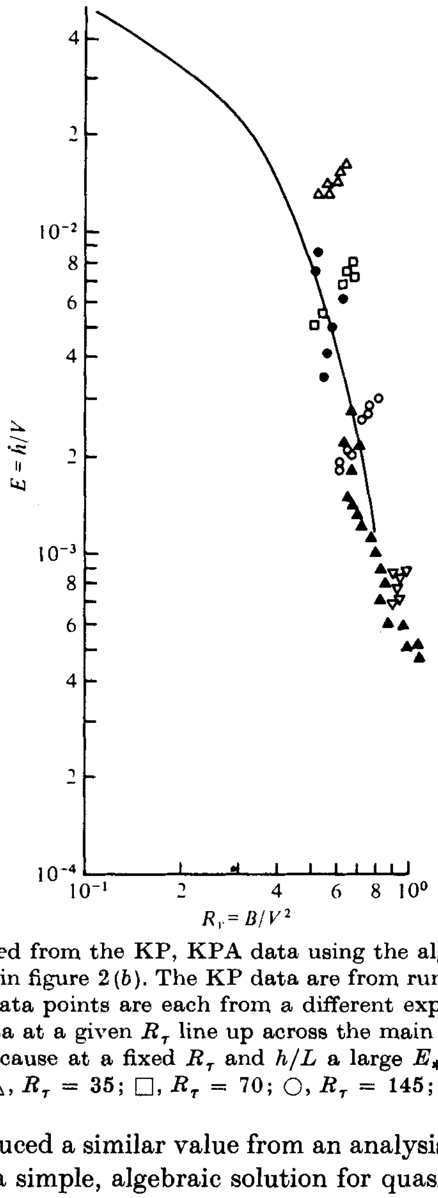

FIGURE 4. $E(R_v)$ computed from the KP, KPA data using the algebraic form of (9). The solid curve is the ET result as in figure 2(*b*). The KP data are from runs 4 and 9 and are for various R_T and h/L. The KPA data points are each from a different experimental run and are all for $h/L = 0{\cdot}5$. The KPA data at a given R_T line up across the main trend of the data (decreasing E with increasing R_v) because at a fixed R_T and h/L a large E_* implies a large R_v. KP: ●, run 4; ▲, run 9. KPA: △, $R_T = 35$; □, $R_T = 70$; ○, $R_T = 145$; ▽, $R_T = 285$.

has independently deduced a similar value from an analysis of KP data. Substitution of (12) into (8) yields a simple, algebraic solution for quasi-steady E_* which is compared in detail with the KP, KPA observations. A breakdown of the approximation $R_v =$ constant occurs at large $R_T h/L$.

It is useful to put aside (8) and recompute the solution to see how the factor n arises. In the linearly stratified case of KP, (3*b*) and (12) give

$$h\dot{V} = h\dot{h}N/(2R_v)^{\frac{1}{2}} = \dot{h}V,$$

hence

$$d(hV)/dt = 2\dot{h}V. \tag{13a}$$

In the two-layer case of KPA, (3*c*) and (12) give

$$\dot{V} = 0,$$

hence

$$d(hV)/dt = \dot{h}V. \tag{13b}$$

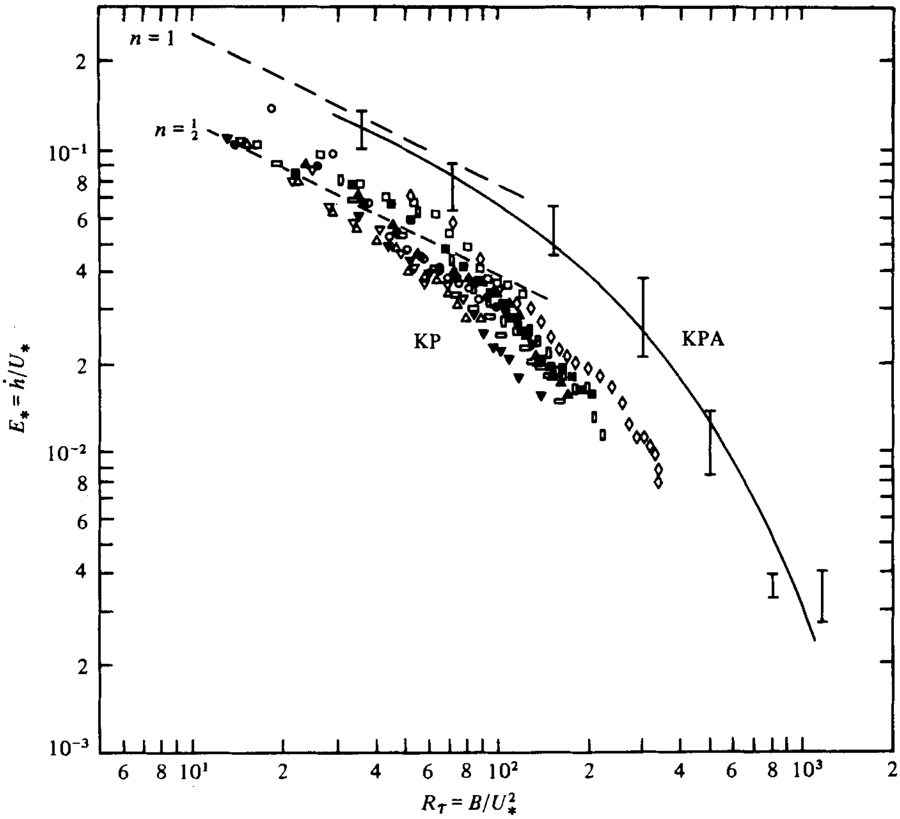

FIGURE 5. Entrainment data from KP and KPA. The KPA curve is their extrapolation to $h/L = 0$. The dashed lines are the small $R_\tau h/L$ approximation of (14), $E_* = nR_v^{\frac{1}{2}}R_\tau^{-\frac{1}{2}}$, where $n = \frac{1}{2}$ or 1 and $R_v = 0{\cdot}6$.

	□	△	○	▽	■	▲	●	▼	◇	▯	▭
ρU_*^2	0·995	1·485	2·120	2·750	0·995	1·485	2·120	2·750	0·995	2·120	2·750
$(\partial\rho/\partial z) \times 10^3$	1·92	1·92	1·92	1·92	3·84	3·84	3·84	3·84	7·69	7·69	7·69

The momentum balance may be written using (13) as

$$n^{-1}\dot{h}V = U_*^2(1-2CR_v^{-1}R_\tau h/L),$$

or solving for E_*,

$$E_* = \dot{h}/U_* = nR_v^{\frac{1}{2}}R_\tau^{-\frac{1}{2}}(1-2CR_v^{-1}R_\tau h/L), \tag{14}$$

where $n = \frac{1}{2}$ or 1 if the fluid has linear or two-layer stratification and $R_v = 0{\cdot}6$ as before. At the same R_τ and h/L, the predicted E_* in the linearly stratified case is half the predicted E_* in the two-layer case. The factor 2 arises because half the available momentum supply (screen stress minus side-wall drag) must be used to accelerate the mixed layer in the linearly stratified case in order to maintain R_v constant as B increases with h [see (3*b*)]. All of the available momentum supply is used to accelerate entrained fluid in the two-layer case, where B is constant (3*c*). Observed screen speeds (discussed below) provide direct evidence that V does significantly increase with h in the linearly stratified case and is quasi-steady in the two-layer case.

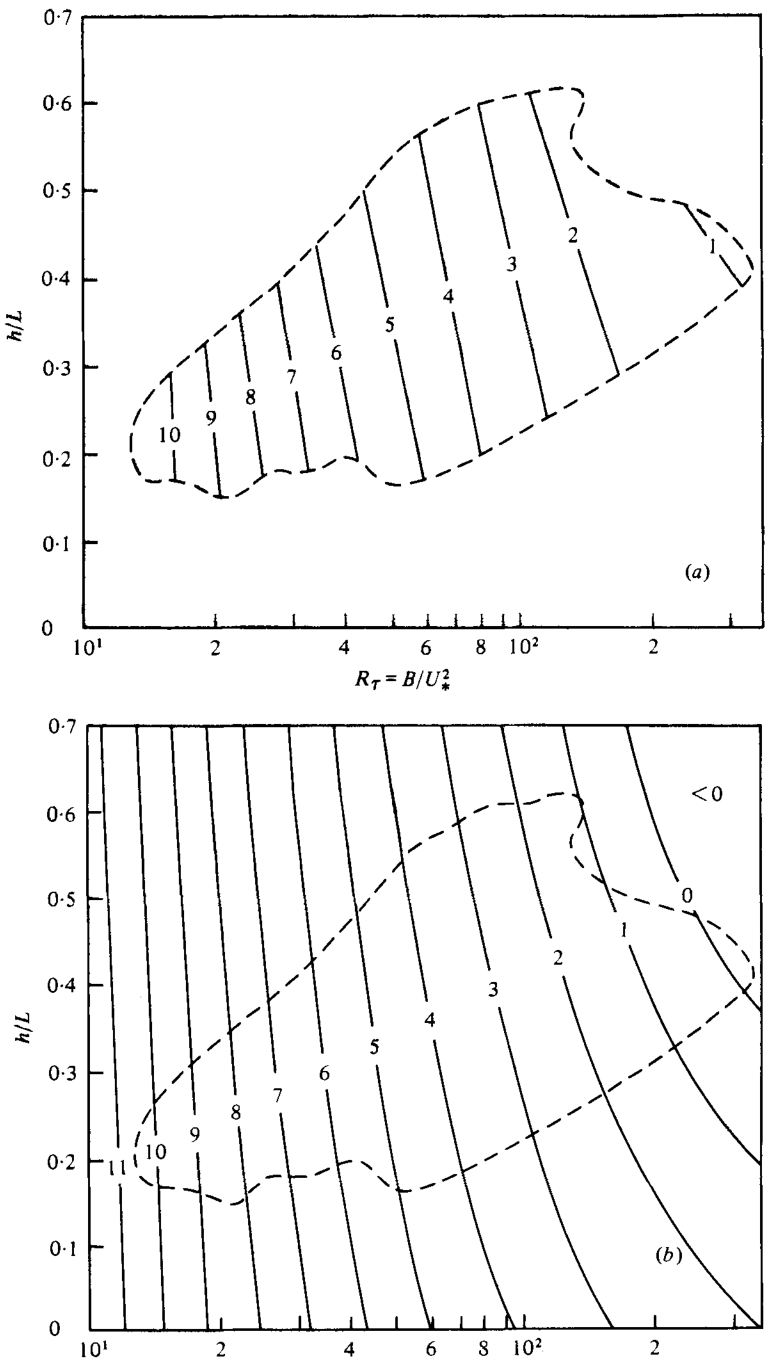

FIGURE 6. (*a*) Observed entrainment rate $E_* = h/U_*$ ($\times 10^2$) from KP as a function of h/L and R_T. (*b*) Entrainment rate ($\times 10^2$) predicted by (14).

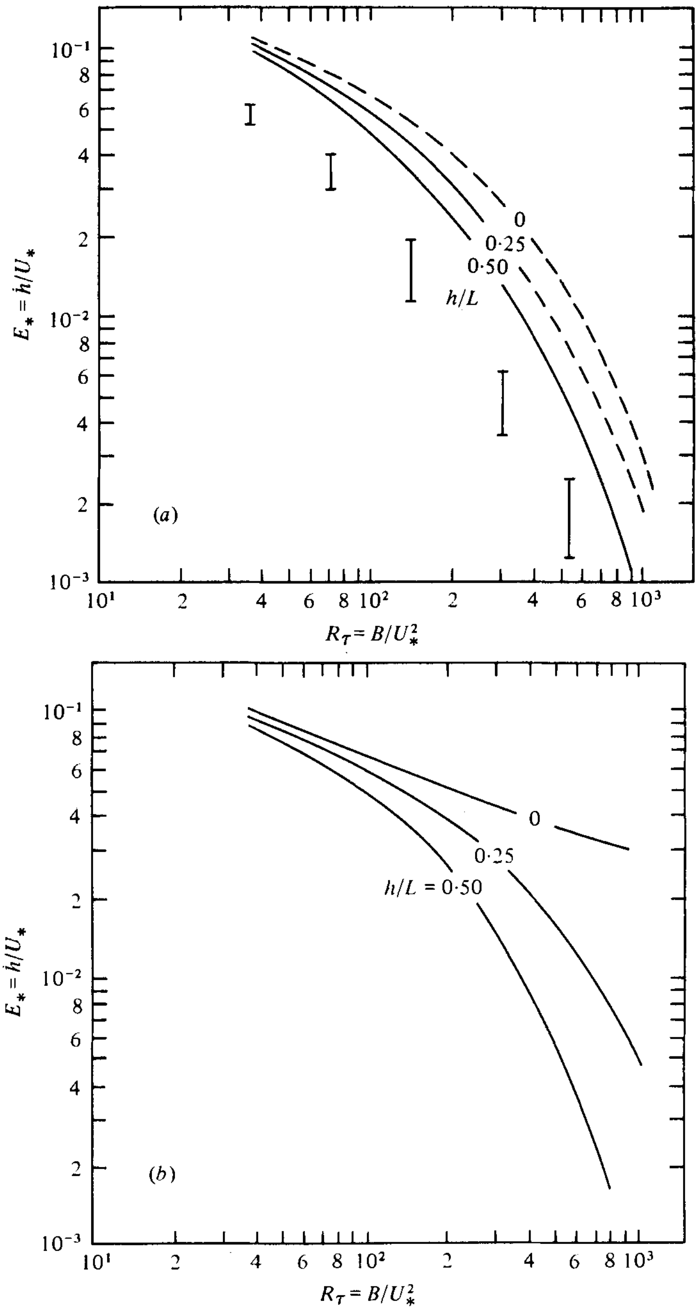

FIGURE 7. (*a*) Entrainment rate E_* from KPA. Solid lines represent observations, dashed lines indicate extrapolations from larger h/L. After Kantha (1975, figures 36, 37, 38). (*b*) E_* at $h/L = 0{\cdot}5$, $0{\cdot}25$, and 0 predicted using (11) as the entrainment law. The predicted R_v exceeds $1{\cdot}0$ on $h/L = 0{\cdot}25$ for $R_\tau > 550$ and on $h/L = 0{\cdot}50$ for $R_\tau > 400$.

In the range $R_\tau h/L < 10$ the side-wall term of (14) is $< 0\cdot1$ and $E_* \simeq nR_v^{\frac{1}{2}}R_\tau^{-\frac{1}{2}}$ (figure 5). The factor n difference in E_* between KP and KPA is clearly present and the data approach $E_* \propto R_\tau^{-\frac{1}{2}}$ at low R_τ. The comparison in figure 5 is a rather sensitive test of the value of R_v. For $R_v = 0\cdot4$–$0\cdot8$, the change in the predicted E_* is as large as the second error bar on the KPA experimental curve. The data indicate that $0\cdot5 < R_v < 0\cdot6$ in the low R_τ regime of both experiments.

For larger $R_\tau h/L$ the side-wall term of (14) reduces entrainment significantly. To see the side-wall effect in the KP experimental data, hold R_τ fixed and then look for the expected variation of E_* with h/L. For fixed R_τ, h is proportional to U_*/N. The experimental run with the largest U_*/N ($\rho U_*^2 = 2\cdot75$ dyne cm^{-2}, $\partial\rho/\partial z = 1\cdot92 \times 10^{-3}$ g cm^{-4}, run 4) has a consistently small E_*; the experimental run with the smallest U_*/N ($\rho U_*^2 = 0\cdot99$ dyne cm^{-2}, $\partial\rho/\partial z = 7\cdot69 \times 10^{-3}$ g cm^{-4}, run 9) has a consistently large E_*. Inspection of figure 5 shows that the KP data cloud is stratified by h/L in the constant-R_τ direction. There are random (apparently) fluctuations of E_* along all the experimental curves, but the amplitude of those fluctuations is small compared with the depth of the data cloud. One experimental run ($\rho U_*^2 = 2\cdot120$ dyne cm^{-2}, $\partial\rho/\partial z = 1\cdot92 \times 10^{-3}$ g cm^{-4}, run 3) breaks decisively from this otherwise neat pattern by having a relatively very high E_* at small R_τ and a relatively small E_* at large R_τ.

The side-wall effect upon E_* is predicted by (14) to increase with R_τ and to be linear in h/L. The increase with R_τ is apparent in figure 5 as the increase in the depth of the data cloud with R_τ. Linearity in h/L (in the $R_\tau h/L$ range where this solution is valid) is apparent in KPA, figures 6 and 7. Both of these properties of the side-wall effect are also apparent in the analysis in § 5. The magnitude of the predicted side-wall effect is close to that observed. At $R_\tau = 100$ (a large R_τ achieved in nearly all of the KP experimental runs), the range of h/L in the data is $0\cdot22 < h/L < 0\cdot60$. From (14), this gives $1\cdot9 \times 10^{-2} < E_* < 3\cdot2 \times 10^{-2}$; the observed range is $2\cdot0 \times 10^{-2} < E_* < 3\cdot4 \times 10^{-2}$, approximately. Hence the observed side-wall effect upon entrainment is consistent with the model developed here, in which side-wall drag serves only to brake the mean flow.

The important h/L dependence suggests that the KP observations be plotted as a function of both R_τ and h/L. The data were digitized from Kantha (1975, figure 40) and the h for each data point was computed from $h = (2R_\tau)^{\frac{1}{2}}\, U_*/N$. Data with large h/L tend to occur at large R_τ (figure 6*a*). When the data are projected upon the R_τ axis as in figure 5, the h/L dependence is biased into R_τ dependence. The data were contoured manually using straight lines. What appeared to be random noise caused some ambiguity in the range $50 < R_\tau < 70$, but the broad features shown in figure 6 (*a*) were well defined. The same field computed from (14) is very similar (figure 6*b*) except at the largest $R_\tau h/L$ achieved in the KP experiment. The similar slope of isolines is another indication that the predicted side-wall effect is similar in magnitude to the observed effect.

According to (14), E_* vanishes when $2CR_v^{-1}R_\tau h/L = 1$, or $\tau_s = \tau_w$, and the side-wall drag absorbs all the imposed stress. For $R_\tau = 200$ this occurs at $h/L = 0\cdot6$. At still larger $R_\tau h/L$, (14) predicts $E_* < 0$, which is physically unrealistic, indicating that the approximate closure $R_v =$ constant has broken down.

Numerical solution for E_*

The entrainment law $E(R_v)$ [equation (11)] must be used as the model closure equation in the large $R_\tau h/L$ regime. R_v is then free to assume a value consistent with the imposed flow parameters and the catastrophe $E_* < 0$ never occurs. The model equations (3), (4) and (11) are integrated numerically as an initial-value problem for h and V, and the solution is differentiated to give $\dot{h}$. Initial conditions are the initial state of an experiment. The solutions tend to be dominated by side-wall drag when $R_v > 1{\cdot}0$. Because of the uncertainties in (6) and because the predicted entrainment is then sensitive to the details of (11), the solutions for $R_v > 1{\cdot}0$ should be regarded sceptically.

The model-predicted E_* is very similar to the KPA results [and to the corresponding approximate solution (14)] at all h/L for $R_\tau \lesssim 150$ (figure 7). The predicted E_* is very similar to the observed E_* at $h/L = 0{\cdot}5$ for all R_τ. (This may be fortuitous because R_v exceeds $1{\cdot}0$ at $R_\tau = 400$ and the solution is not considered reliable at larger R_τ.) The model-predicted E_* at $h/L = 0{\cdot}25$ exceeds the corresponding KPA extrapolation at large R_τ, and the prediction at $h/L = 0$ greatly exceeds the KPA extrapolation. This discrepancy arises at least in part because E_* becomes nonlinear in h/L in the regime dominated by side-wall drag. This is apparent in the numerical solutions and in the KPA data as the decrease in the slope $\partial E_*/\partial(h/L)$ at large $R\tau\, h/L$ (see Kantha, 1975, figures 31, 32, 33; or KPA, figures 6, 7). Model solutions indicate that nonlinearity is substantial for $R_\tau h/L \gtrsim 150$; at $R_\tau = 264$, $\partial E_*/\partial(h/L)$ decreases by a factor of 2 as h/L increases from $0{\cdot}3$ to $0{\cdot}6$. As a consequence, the KPA linear extrapolation of E_* to $h/L = 0$ using observations made at very large R_τ in the range $0{\cdot}35 < h/L < 0{\cdot}5$ would be expected to consistently and significantly underestimate the true value of the entrainment. (An extrapolation using KP data is discussed in the next section.)

The predicted E_* at $h/L = 0$ deviates slightly from $E_* \propto R_\tau^{-\frac{1}{2}}$ because R_v increases with R_τ: at $R_\tau = 35$, $R_v = 0{\cdot}55$; at $R_\tau = 800$, $R_v = 0{\cdot}80$. Hence the value of the appropriate R_v in (12) depends weakly upon R_τ even in the absence of side-wall drag.

Screen velocity observations and mean-velocity predictions

Neither KP nor KPA made accurate measurements of the mean velocity. They did measure the screen velocity U_s and KP noted that the mean velocity was 'typically about half that of the screen'. Kantha (1975) noted that

$$0{\cdot}5 < V/U_s < 0{\cdot}7, \tag{15}$$

which is used here to compare the predicted V with the observed U_s.† This comparison is useful despite the imprecision of (15) because the time dependence of U_s and V is qualitatively different in the two-layer and linearly stratified cases. In the two-layer case, U_s increases rapidly during the transient period at the beginning of an experimental run and then slowly decreases and approaches an asymptotic value from above (figure 8). In the linearly stratified case, U_s increases monotonically and approaches an asymptotic value from below (figure 9). The increase or decrease of U_s

† It is expected that U_s will be roughly proportional to V in these experiments if $\tau_s \propto (U_s - V)^2$, and not simply $\tau_s \propto U_s^2$.

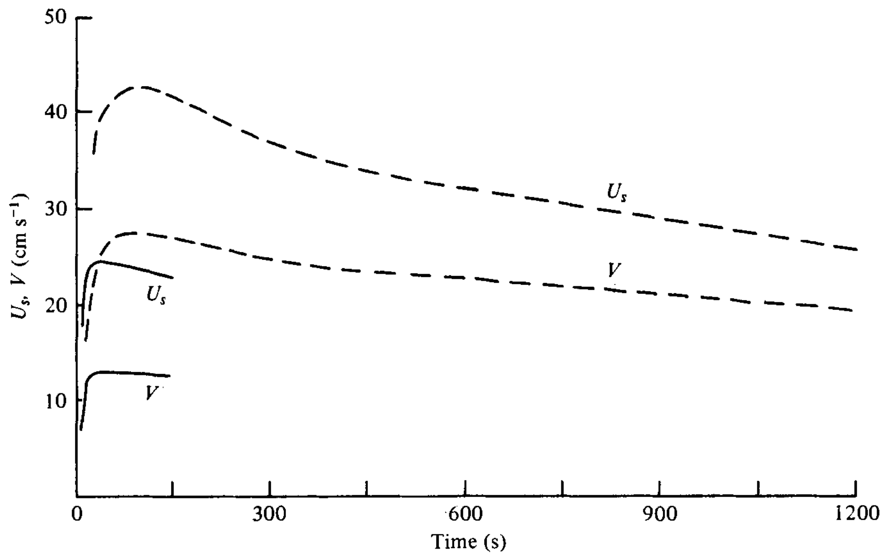

FIGURE 8. Observed U_s and predicted V for the KPA two-layer case. In both experimental runs $\tau_s = 2{\cdot}0$ dyne cm^{-2}; they differ in having $B = 524$ cm^2 s^{-3} ($R_T = 262$, dashed line) and $B = 72$ cm^2 s^{-3} ($R_T = 36$, solid line). The aspect ratio h/L was about 0·2 at the beginning and 0·9 at the end of both experimental runs. The predicted R_v exceeds 1·0 in the run $B = 524$ cm^{2}s^{-3} at $t = 550$ s.

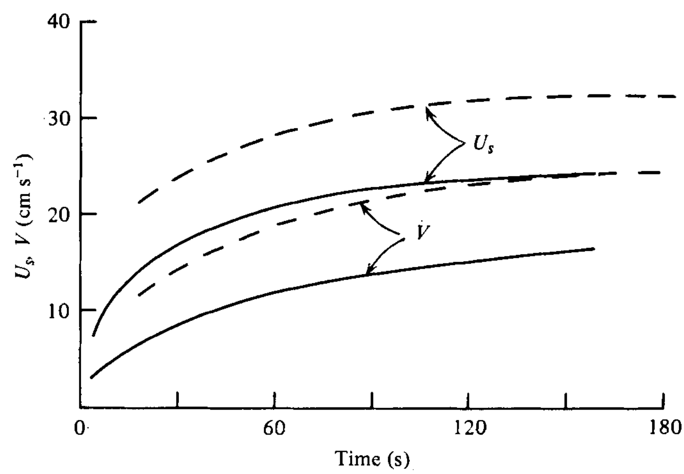

FIGURE 9. Observed U_s and predicted V for the KP linearly stratified case. Experimental runs are for $\tau_s = 2{\cdot}75$ dyne cm^{-2} and $\partial\rho/\partial z = 7{\cdot}69 \times 10^{-3}$ g cm^{-4} (dashed line); $\tau_s = 1{\cdot}49$ dyne cm^{-2} and $\partial\rho/\partial z = 3{\cdot}84 \times 10^{-3}$ g cm^{-4} (solid line).

(apart from the initial transient in the two-layer case) can be due only to the different forms of stratification.

In two experimental runs reported by KPA ($R_T = 36$, 262), τ_s was the same but U_s was greater by a factor of almost 2 in the run with $R_T = 262$ (figure 8). This is consistent with the previous analysis, which showed that R_v will be nearly the same in the two runs, hence large B requires large V ($V \sim B^{\frac{1}{3}}$) and thus large U_s. The ratio (predicted V/observed U_s) is approximately 0·5–0·7, consistent with (15).

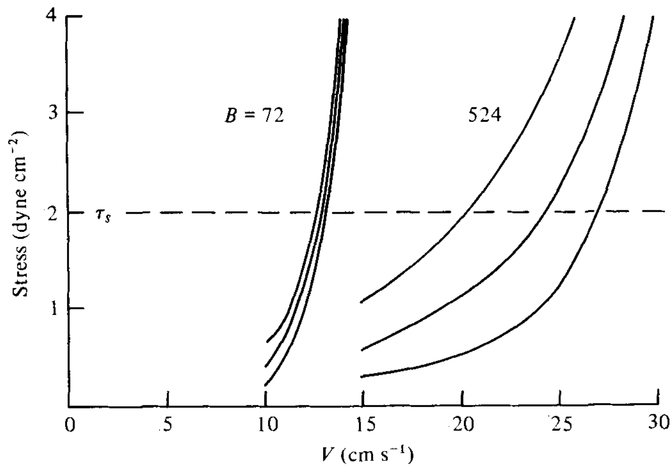

FIGURE 10. Sum of entrainment stress and side-wall drag for the KPA experimental runs of figure 9 evaluated at (from left to right) $h/L = 0{\cdot}9$, $0{\cdot}5$, $0{\cdot}2$. The imposed stress was $2{\cdot}0$ dyne cm^{-2}.

After the initial acceleration of V the momentum balance in the two-layer case is approximately

$$U_*^2 = \dot{h}V + 2CV^2h/L, \tag{16}$$

where the term $\dot{h}V$ is called the entrainment stress. From (11), $\dot{h}V = 5 \times 10^{-4}\, V^{10}B^{-4}$, and the entrainment stress may be thought of as a highly nonlinear form of bottom drag. For $R_\tau = 36$ the entrainment stress dominates the right-hand side of (16) ($R_\tau h/L \lesssim 30$), which therefore increases very steeply with V in the neighbourhood $V \simeq (B/0{\cdot}6)^{\frac{1}{2}}$ (figure 10), hence V changes only slightly as h/L increases from $0{\cdot}2$ to $0{\cdot}9$. For $R_\tau = 262$ the side-wall drag balances a significant fraction of the screen stress and V must decrease substantially as h/L and the side-wall drag increase. The mean velocity approaches an asymptotic value from above as the side-wall drag approaches the magnitude of the screen stress.

For the two extreme experimental runs reported by KP (predicted V/observed U_s) is again $0{\cdot}5$–$0{\cdot}7$. B increases with time in the linearly stratified case, hence V must also increase in order for R_v to remain within the range $R_v \lesssim 1{\cdot}0$ where the entrainment stress can partially balance the screen stress. As h/L and the side-wall drag increase, $\dot{h}$ and $\dot{V}$ decrease and V approaches an asymptotic value from below.

The predicted V reaches a maximum approximately in phase with U_s in both experimental runs of figure 8. The same approximate phase consistency is found in mixed-layer depth (figure 3), indicating that the model predicts the onset of entrainment, a time-dependent phenomenon, with at least some success. However, the model prediction is less than perfect. The predicted h lags, closely matches and leads the observed h in figures 3(*a*), (*b*) and (*c*). The phase discrepancy (when it occurs) appears to arise mainly during the initial transient period and then persists throughout an experimental run. The entrainment velocity and the rate of change of R_v at later times are predicted rather well in all three cases. The KPA experiment was not intended to study time-dependent entrainment, hence this discrepancy may not be significant; it is of small amplitude in any event. Nevertheless, it does appear

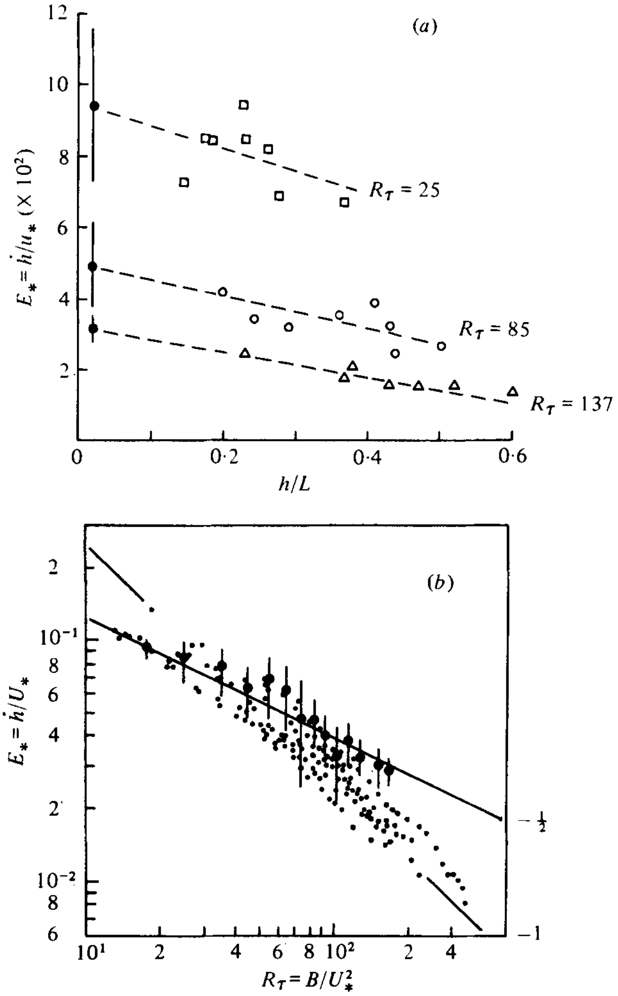

FIGURE 11. (a) Non-dimensional entrainment rate $E_* = \dot{h}/U_*$, from KP as a function of h/L for $R_\tau = 25 \pm 5$, 85 ± 5 and $137 \pm 7{\cdot}5$. The dashed lines are least-squares fits to the data. The intercepts at $h/L = 0$ are shown with error bars equal to ± 2 times the square root of the estimated variance of the intercept, roughly 90 % confidence limits. (b) Extrapolation of E_* to $h/L = 0$. The lines are $E_* = 2{\cdot}5\, R_\tau^{-1}$ (-1) and $E_* = nR_v^{\frac{1}{2}} R_\tau^{-\frac{1}{2}}$ with $n = \frac{1}{2}$ and $R_v = 0{\cdot}6$ ($-\frac{1}{2}$).

to be systematic and may be a hint that the entrainment rate in these experiments has a dependence, albeit weak, upon a parameter other than R_v. Further experiments which include precise measurements of V are required to explore this question.

5. Extrapolation of E_* to $h/L = 0$

The side-wall effect upon E_* is predicted and observed to be linear in h/L over a substantial portion of the parameter range covered in the experiments, roughly $R_\tau h/L \lesssim 75$. Over that range the data may be used to compute E_* at $h/L = 0$ by an objective, linear extrapolation. The KP data are best suited for this purpose because they are continuously distributed in R_τ (figure 1b). The data were grouped by R_τ ($\Delta R_\tau = 10$ if $R_\tau < 125$, $\Delta R_\tau = 15$ if $R_\tau > 125$) and the data within each group were interpolated to the central value of R_τ to remove R_τ dependence. (The anomalous experimental run noted above (no. 3) was deleted.) A straight line was least-squares fitted to the data $E_*(h/L)$ in each group (figure 11*a*). The number of points in a group varied from a maximum of 10 to a minimum of 4. Hence the magnitude of the cross-correlation between E_* and h/L was somewhat unstable but generally exceeded 0·5 if $R_\tau < 125$ and 0·8 if $R_\tau > 125$.

The extrapolation of E_* to $h/L = 0$ falls near the corresponding model prediction $E_* = nR_v^{\frac{1}{2}}R_\tau^{-\frac{1}{2}}$ ($n = \frac{1}{2}$, $R_v = 0{\cdot}6$) over the full range of R_τ with a sufficient data density for this analysis ($17 < R_\tau < 160$; figure 11*b*). At very small R_τ the side-wall effect is negligible and the extrapolated E_* falls within the data cloud and well below the line $E_* = 2{\cdot}5\,R_\tau^{-1}$. At large R_τ the extrapolated E_* is well defined and is clearly above the line $E_* = 2{\cdot}5\,R_\tau^{-1}$. The greatest discrepancy occurs near $R_\tau = 60$, where there appears to be a hole in the data cloud, perhaps due to a superposition of random errors (three experimental runs have E_* rather high in that range of R_τ).

Note that the KPA extrapolation of E_* to $h/L = 0$ (figure 5) is also consistent with $E_* \propto R_\tau^{-\frac{1}{2}}$ up to $R_\tau \simeq 145$. The next data at $R_\tau \simeq 280$ fall below $E_* \propto R_\tau^{-\frac{1}{2}}$ but are in the range where E_* is nonlinear in h/L.

The result $E_* \propto R_\tau^{-\frac{1}{2}}$ is a statement of momentum conservation, subject to $R_v \simeq$ constant (approximately independent of time and of R_τ). Mean momentum conservation is thus a key constraint upon the entrainment rate in these experiments. This has considerable significance for application of the KP, KPA results; a mean momentum constraint may lead to entrainment predictions very different from those of the turbulent energy constraint suggested by $E_* \propto R_\tau^{-1}$.

6. Conclusion and remarks

In an ideal experiment in which B and U_* are constant, h/L vanishes and no time scale is relevant, the dimensional analysis that requires $\dot{h}$ to be constant (§ 1) requires V to be constant as well. Hence

$$V = U_* F(R_\tau), \tag{17}$$

where F is some function of R_τ alone,† and the ideal experiment could be scaled equally well with U_* or V. The ideal experiment is, therefore, a degenerate case. The KP, KPA experiments considered together were not degenerate because B varied with h in a different way in the two experiments and because h/L was finite and variable in both experiments. These variations of B and h/L caused systematic departures from (17). They also caused significant corresponding variations in the entrainment rate E_* which are easily understood provided that we are aware of the entrainment law $E(R_v)$ of figure 4: the difference in $B(h)$ causes a difference of a factor of 2 in E_* between KP and KPA and the closely related difference in screen speed behaviour; the finite aspect ratio h/L allows momentum loss to the side walls and a consequent decrease in E_*.

Time dependence can dramatically break the degeneracy implied by (17). Consider reversing the direction of the imposed stress during the course of an experiment. Given $E_*(R_\tau)$ the effect upon entrainment can only be guessed. Given the $E(R_v)$ in figure 4 and the momentum conservation equation a definite prediction can be made; entrainment would strongly decrease as V decreased (R_v increased) and would recover

† R_v must also be constant in time in the ideal experiment but may depend upon R_τ.

to its former magnitude only as V recovered. Assuming that the stress reversal occurs when $h = 10$ cm in the case of figure 3(*b*), the time during which entrainment would be depressed is expected to be $2h(B/R_v)^{\frac{1}{2}}/U_*^2 \simeq 150$ s and easily observable. A generalization of this is a stress which has a steady component and a fluctuating component which reverses rapidly compared with the response time of the mean flow.

It is unifying to learn that the KP, KPA experiments follow an entrainment law common to the wind-driven ocean surface mixed layer and to a surface half-jet. These flows differ greatly in the way in which they are driven. It appears that they are in a regime in which the supply of mean momentum, and not some property of the turbulence within the mixed layer, is the most important constraint upon the entrainment rate. The observed side-wall effect upon entrainment and the observed $E_* \propto R_\tau^{-\frac{1}{2}}$ behaviour provide additional support for this conclusion.

There are limiting cases where a mean momentum constraint is obviously not relevant. Entrainment occurs in the grid-stirred experiments of Turner (1968) in the absence of a mean flow. There is no entrainment in the buoyancy-driven two-layer shear-flow experiments of Thorpe (1973) because there is no significant source of turbulence within the homogeneous layers. Further observations are needed to unravel the complementary roles of mean flow shear and turbulence in the important intermediate case of a mean flow driven by a stress. There is no indication from this analysis that the finite aspect ratio of the laboratory tank is a fundamental drawback. Experiments of the KP, KPA type which include measurements of the mean and turbulent velocities and generalized forcing are thus expected to be an important element in the further study of entrainment.

I have enjoyed many interesting discussions of entrainment experiments with Professor Claes Rooth. Thanks go to Professor Owen Phillips, Dr Christopher Mooers and Dr Barry Lesht for their valuable comments and to Ms Michelle McDowell for her help in preparing the manuscript. This work was begun at the Rosenstiel School of Marine and Atmospheric Science, University of Miami, with graduate research assistantship support from NSF grant GA-34009. Computing resources were provided in part by the University of Rhode Island Academic Computing Center.

REFERENCES

Ellison, T. H. & Turner, J. S. 1959 Turbulent entrainment in stratified flows. *J. Fluid Mech.* **6**, 423–448.

Kantha, L. H. 1975 Turbulent entrainment at the density interface of a two-layer stably stratified fluid system. *Dept. Earth Planet. Sci., Johns Hopkins Univ. Rep.* GFDL TR 75-1.

Kantha, L. H., Phillips, O. M. & Azad, R. S. 1977 On turbulent entrainment at a stable density interface. *J. Fluid Mech.* **79**, 753–768.

Kato, H. & Phillips, O. M. 1969 On the penetration of a turbulent layer into stratified fluid. *J. Fluid Mech.* **37**, 643–665.

Lofquist, K. 1960 Flow and stress near an interface between stratified fluids. *Phys. Fluids* **3**, 158–175.

Mellor, G. L. & Durbin, P. A. 1975 The structure and dynamics of the ocean surface mixed-layer. *J. Phys. Ocean.* **5**, 718–728.

Moore, M. J. & Long, R. R. 1971 An experimental investigation of turbulent stratified shearing flow. *J. Fluid Mech.* **49**, 635–655.

PHILLIPS, O. M. 1977 Entrainment. In *Modelling and Prediction of the Upper Layers of the Ocean* (ed. E. B. Kraus), chap. 7. Pergamon.

POLLARD, R. T., RHINES, P. B. & THOMPSON, R. O. R. Y. 1973 The deepening of the wind-mixed layer. *Geophys. Fluid Dyn.* **3**, 381–404.

PRICE, J. F., MOOERS, C. N. K. & VAN LEER, J. C. 1978 Observation and simulation of storm-driven mixed-layer deepening. *J. Phys. Ocean.* **8**, 582–599.

SCHLICHTING, H. 1968 *Boundary Layer Theory*. McGraw-Hill.

THORPE, S. A. 1973 Experiments on instability and turbulence in a stratified shear flow. *J. Fluid Mech.* **61**, 731–751.

TURNER, J. S. 1968 The influence of molecular diffusivity on turbulent entrainment across a density interface. *J. Fluid Mech.* **33**, 639–656.

TURNER, J. S. 1973 *Buoyancy Effects in Fluids*. Cambridge University Press.